Academic Journal of Science and Technology
ISSN: 2771-3032 | Vol. 9, No. 1, 2024

Lightweighting Study of Rotary Kiln Cylinder Structure Based on Response Surface

Tao Peng*, Huailin Luo and Zhaoxi Wang

Sichuan University of Light and Chemical Technology School of Mechanical Engineering, Yibin City, Sichuan Province Zip Code 644000, Chiha

*Corresponding author: Tao Peng (Email: 1574579067@qq.com)

Abstract: To achieve the lightweight design of the rotary kiln cylinder, reduce its manufacturing costs, and improve its mechanical properties, the maximum stress and deformation were determined through a static and thermal structural analysis of the rotary kiln equipment. Employing the Box-Behnken response surface method, an optimization of the rotary kiln cylinder structure was performed, with the aim of minimizing the cylinder mass and deformation, while considering constraints such as cylinder thickness and yield strength. A multi-objective optimization mathematical model was established, and three sets of Pareto solutions were obtained using a multi-objective genetic algorithm. The optimized design of thickness structure was determined for the stall section, transition section, and cylinder section of the rotary kiln. The finite element method was utilized to simulate the optimized solutions and verify their validity and accuracy. The results showed that the rotary kiln cylinder mass was reduced by 13.8%, and the maximum deformation under static structural conditions was reduced by 4.6%, while maintaining the strength requirement of the structural stiffness. The relevant geometric parameters of the optimal solution were verified by finite element numerical tests, and the optimized cylinder mass, maximum stress and deformation under static structural conditions, and maximum deformation and stress under thermal structural coupling were in good agreement with the numerical test results, with a deviation of less than 2%. Additionally, this study realized the lightweight design of the rotary kiln cylinder and provided useful references for the thickness design of the rotary kiln cylinder.

Keywords: Response surface, Multi-targeting, Lightweighting, Genetic Algorithm.

1. Introduction

The rotary kiln is widely used in cement, metallurgy, building materials, and environmental protection industries. It plays a vital role in the production and processing process. The manufacturing and maintenance costs of rotary kilns directly impact the overall cost-effectiveness of the production equipment. Numerous scholars both domestically and internationally have conducted extensive research on optimizing rotary kiln equipment. For instance, Xiao Yougang et al. [1] established an unsteady-state heat transfer model for the kiln wall. The results showed that thicker kiln skins result in smaller radial temperature gradients, reducing thermal stress. Controlling the kiln skin thickness at 252mm can maintain the outer surface temperature of the rotary kiln at 200 degrees. Li Zhigang [2] studied the deviation of the cylinder axis from the theoretical axis during the operation of the rotary kiln. This deviation results in uneven forces on various components and increased wear on moving parts. By adjusting variables such as gear pitch, initial deformation of the rollers, kiln adjustment amount, and support angle, the optimal design for the coaxial equal-carrying rotary kiln can be achieved. Yang Wei [3] established a steady-state heat transfer mathematical model based on the flow field and temperature distribution inside the rotary kiln. They analyzed the influence of diameter change size and location on kiln temperature to obtain the optimal diameter change for the rotary kiln, aiming to improve the material conversion rate. Chen Mingfei [4] analyzed the stresses and deformations of the cylinder, identified hazardous sections, and proposed the adjustment of support spans. Li Yanmin [5] optimized the number of support gears for a specific rotary kiln equipment and verified the feasibility of this scheme theoretically using ANSYS analysis. Lei Xianming [6-7] focused on the discontinuous multi-contact system of the rotary kiln. They established a discontinuous multi-body contact model for the cylinder and roller ring, analyzed the stress and deformation of the cylinder, and carried out improvements in the cylinder structure to reduce the maximum equivalent stress. To address issues related to unclear stress and unreasonable strength distribution in the rotary kiln cylinder, an improved multi-objective genetic algorithm was applied. This algorithm considered constraints such as cylinder thickness, cross-section deformation, and deflection, conducting a comprehensive search in the given design space to determine the optimal cylinder thickness. Qiao Bin [8] analyzed the factors influencing the design of large-span rotary kilns. They proposed improving the three-stage rotary kiln to a two-stage design, which saves manufacturing costs but increases overall cylinder deformation. The weight and production cost of the cylinder are determined by its thickness. The traditional cylinder thickness design may be unreasonable, as the cylinder operates under heavy loads, which can easily lead to deformation and cracking. Therefore, conducting research on the thickness of the rotary kiln cylinder is highly significant for ensuring the smooth operation of the entire rotary kiln equipment.

2. Finite Element Analysis of Rotary Kiln Model

2.1. Rotary kiln material performance parameters

The research focused on the $\phi 2.75 \times 50.95m$ calcined rotary kiln, and Table 1 shows the material parameters for

each part of the rotary kiln barrel and refractory bricks. The cylinder has an inclination angle of 2.977°, and the mass of the refractory brick layer inside the cylinder is 199030.7 kg, while the material mass 11000 kg. The densities of the cylinder and refractory bricks at the large gear and at the end of the kiln are equivalent densities that have considered the gravitational impact of other accessories in their locations. Thus, this calculation is an equivalent simplification of the gravitational loads of various accessories [9].

Table 1. Material parameters table

Selected materials	Elastic modulus E(MPa)	Poisson ratio σ	Equivalent density $\rho\,(\mathrm{kg}/mm^3)$	Thermal conductivity W/(m.k)	Thermal expansion coefficient $(\mathrm{a}\times10^{-6}K)$
Barrel (Q345C)	2.01×10^5	0.294	7.85×10^{-6}	48.85	1.06
Barrel at large gear ring (Q345C)	2.01×10^5	0.294	4.096×10^{-5}	48.85	1.06
Cylinder at the end of the kiln (Q345C)	2.01×10^5	0.294	1.32×10^{-5}	48.85	1.06
Refractory bricks (Mullite)	15×10^5	0.22	2.146×10^{-6}	0.23	4.2
Rolling circle (ZG35GrMo)	2.09×10^5	0.291	7.86×10^{-6}	50	13.09
Pallet (ZG35GrMo)	2.09×10^5	0.291	7.86×10^{-6}	50	13.09

2.2. Finite element model analysis

Given the focus on the stress and deformation of the barrel, the wheel belt modeling was simplified to consider full contact between the roller ring and the barrel. However, this is not the actual state; the wheel belt does not make full contact with the surface of the barrel and discontinuous pads exist in the middle. A three-dimensional software was used to create the geometric model for the rotary kiln, as shown in Figure 1.

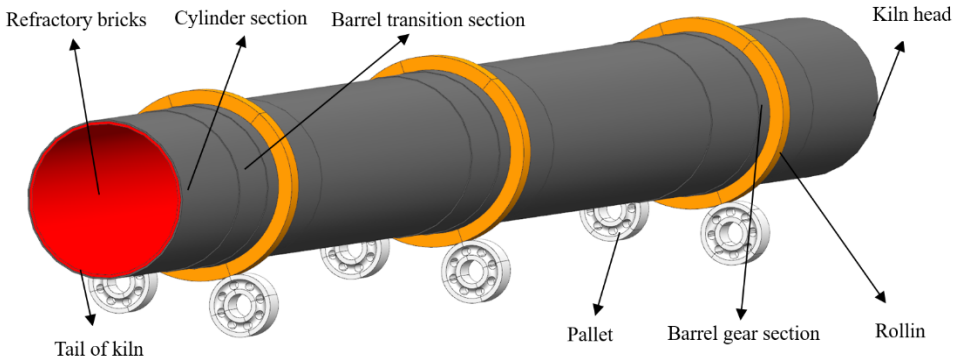

Figure 1. Geometric model of rotary kiln

The rotary kiln barrel is formed by rolling and welding three different thickness segments of steel plates automatically. The maximum wall thickness at the wheel belt support position ensures that the barrel maintains sufficient strength and stiffness. The traditional design has the following cylinder thicknesses: 40mm for the gear section, 32mm for the transition section, and 20mm for the remaining cylinder section. Given the varying internal temperatures of the kiln head and middle cylinder section, the highest temperature is used as the internal temperature of the cylinder for thermal structure coupling analysis.

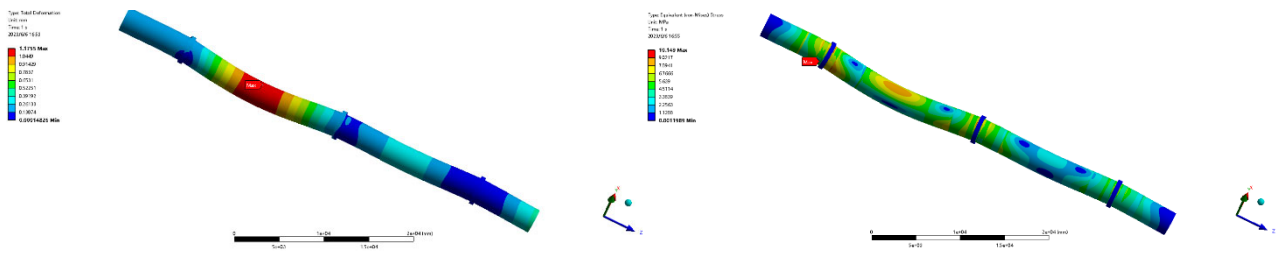

Figure 2. Maximum deformation and maximum equivalent force of static structure

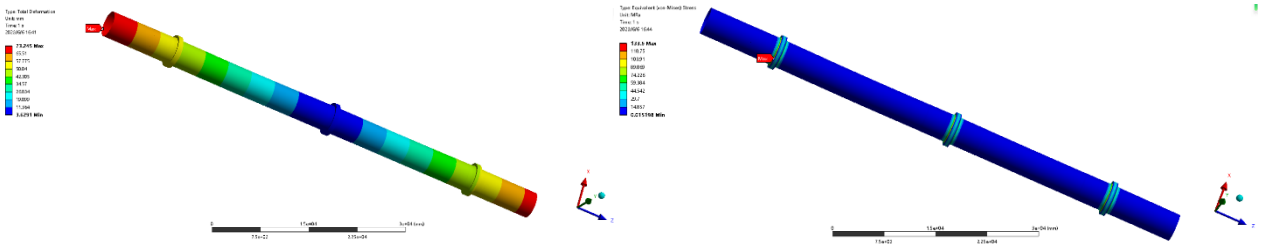

Figure 3. Maximum deformation and maximum equivalent force under thermal structural coupling

The whole model of rotary kiln is used as the object of study for finite element calculation, and the cylinder is taken for analysis as follows: Figure 2 shows the strain and stress cloud diagrams of the rotary kiln cylinder model in the static structure, and it can be seen from the diagram that the cylinder has the largest deformation in the middle of the 2nd and 3rd roller ring, with the maximum deformation of 1.1755 mm , and the maximum equivalent force occurs on the surface of the cylinder under the 3rd roller ring, with the maximum equivalent force of 10.149 MPa . Figure 3 shows the strain and stress cloud diagrams of the rotary kiln cylinder model in the thermal structure coupling field, respectively, and it can be seen that the maximum stress occurs on the surface of the cylinder in the third gear with a value of 133.6 MPa , and the maximum deformation occurs at the end of the cylinder with a value of 73.245 mm . From the comparison of the above data, it can be seen that the temperature has a great influence on the strain and stress of the whole rotary kiln, and this factor needs to be taken into account in the optimization process.

3. Response Surface Optimization

3.1. Response surface model construction

Based on the method provided in the literature for constructing response surface models, the model is formulated using a response surface polynomial of order 2:

$y(x) = a_0 + \sum_{i=1}^{n} a_i x_i + \sum_{i=1}^{n} b_i x_i^2 + \sum_{j=2}^{n} \sum_{i=1}^{j-1} c_i x_i x_j$ in the formula:

$y(x)$ is the target value; x_i , x_j is the design variable; i =1, 2….., a_0 , a_i , b_i , c_i is the coefficient to be determined;

3.1.1. Determination of the optimization model

Barrel thickness is the main geometric parameter affecting the quality of the barrel. In order to reduce the manufacturing cost of the barrel, the thickness of the same section of the barrel is no longer varied according to the design rules. The diameter of the barrel section is written as d ,the diameter of the transition section is j ,and the diameter of the gear section is g ,which is written uniformly as a X vector ,as the design variable of the barrel mass.

$$X = \{ d \ , j \ , g \ \}$$

The main objective of rotary kiln barrel optimization is to achieve the lightweight of rotary kiln barrel, i.e., to reduce the mass while ensuring the strength of the structure, i.e., the lightest mass of rotary kiln and the smallest deformation as the objective function, to ensure that the equivalent force on the barrel is less than the yield strength of the material, and the thickness of each gear section, barrel section and transition section are between the upper and lower limits. Let the mass be $D(x)$, the maximum deformation of the cylinder under the thermal structure coupling is $S(x)$, and the maximum deformation of the static structure cylinder is $M(x)$, the unit is kg and mm respectively. according to the constraints and optimization objectives, the optimization mathematical model of rotary kiln cylinder structure is established as follows.

$$\begin{aligned} &\min \{ D(x), \ S(x), \ M(x) \} \\ &\sigma \le \sigma_{\max} \\ &d^l \le d \le d^u \\ s.t \quad &g^l \le g \le g^u \\ &j^l \le j \le j^u \end{aligned}$$

σ , $\sigma_{\max}$ is expressed as the maximum stress after optimization and the yield strength of this barrel material

d^l , d^u Indicates the upper and lower limits of the cylinder section diameter j^l , j^u Indicates the upper and lower limits of the transition section diameter g^l , g^u Indicates the upper and lower limits of the gear segment diameter

3.1.2. Experimental design for constructing the mode

There are various methods of experimental design, and considering the economy of experimental design, high efficiency and applicability of structural optimization analysis, the Box-Behnken Design experimental design method with high fitting accuracy in Design-Export optimization analysis software is used for experimental design and analysis [10]. There are three levels of each selected design variable in the BBD experimental design, which are indicated by -1, 0, and +1. Combined with the thickness of this rotary kiln cylinder, the range of values of rotary kiln design variables is shown in Table 2.

Table 2. Range of values of rotary kiln design

Variables	Diameter of cylinder section / mm	Transition section diameter / mm	Gear section diameter / mm
-1	2770	2794	2818
0	2780	2804	2824
+1	2790	2814	2830

Appropriate test sample points were selected according to

the range of different design variables, and group test scenarios were derived. Finite element calculations were performed for each group scenario using Ansys to obtain the structural displacement and stress results of the rotary kiln, and the structure weight was calculated using mathematical formulas, and the calculated results are shown in Table 3.

Table 3. Simulation calculation results

Serial number	Diameter of cylinder section d / mm	Transition section diameter j / mm	Gear segment diameter g / mm	Quality (kg)	Maximum barrel deformation under thermal structure coupling (mm)	Maximum deformation of the cylinder under static structure (mm)
1	2770	2814	2824	129560	73.495	2.4712
2	2770	2804	2830	121270	73.467	2.4525
3	2780	2814	2830	142790	73.329	1.6142
4	2790	2804	2830	145140	73.263	1.1527
5	2780	2814	2818	140170	73.347	1.6092
6	2780	2794	2830	123610	73.288	1.564
7	2790	2794	2824	134250	73.316	1.1218
8	2770	2804	2818	118640	73.486	2.4468
9	2790	2804	2818	142520	73.299	1.1484
10	2790	2814	2824	153440	73.255	1.1673
11	2780	2804	2824	131870	73.32	1.5769
12	2770	2794	2824	110380	73.448	2.414
13	2780	2794	2818	120990	73.309	1.5588

3.2. Response surface model building and testing

3.2.1. Response surface model building

Response surface is a visual optimization algorithm that bifurcates the response curves established using the response surface method, and finally obtains the variation law of the response value with the factors and the optimized parameter region. In this study, the barrel section thickness d, transition section thickness j, and gear section thickness g were selected as the variable factors, mass, and maximum displacement as the response targets. Using the Design-Expert software, the Box-Behnken response surface design experiment and analysis, the quadratic response surface model of, can be obtained, as in equation (1), (2), (3):

$$\begin{aligned} D(x) &= 1.319E05 + 11937.50A \\ &+ 9591.25B + 1311.25C + 2.5AB \\ &- 2.5AC + 20A^2 + 17.5B^2 + 2.5C^2 \end{aligned} \tag{1}$$

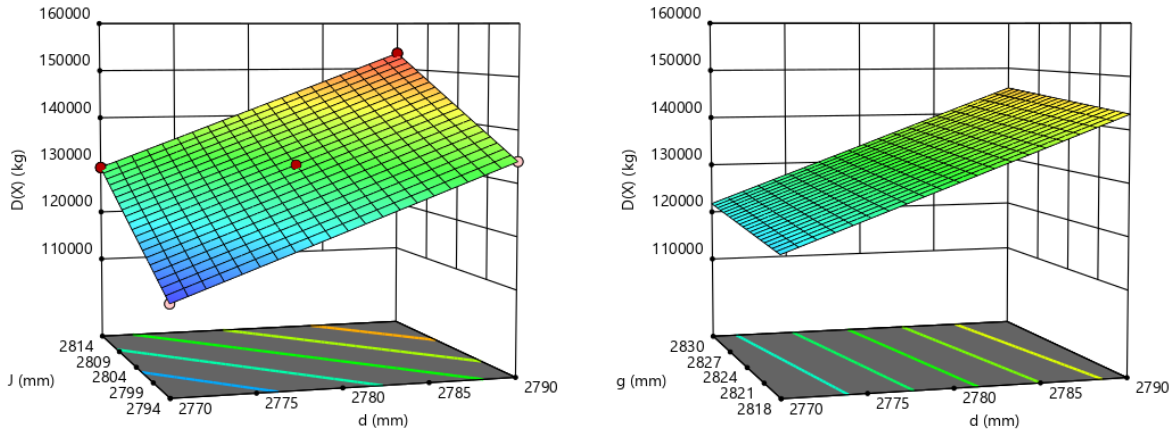

Figure 4. Graph of relationship between design parameters and mass

As shown in Figure 4, it can be observed that the barrel mass increases with an increase in the barrel section diameter, but decreases with an increase in the transition section diameter. This effect has a significant influence on the barrel mass. Moreover, the barrel mass increases with an increase in the diameter of the blocking section, but the effect is not prominent

$$\begin{aligned} S(x) &= 73.32 - 0.0954A + 0.0081B - 0.0118C \\ &- 0.027AB - 0.0042AC + 0.0008BC \\ &+ 0.0595A^2 - 0.001B^2 - 0.0008C^2 \end{aligned} \tag{2}$$

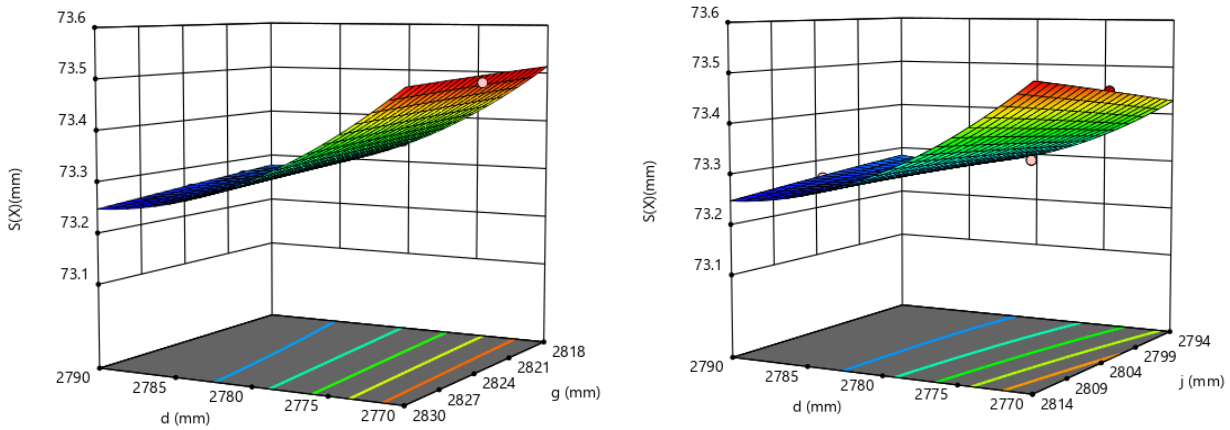

Figure 5. Relationship between design parameters and barrel deformation under thermal structural coupling

From Figure 5, it can be seen that the barrel deformation decreases as the diameter of the barrel section increases, and the diameter of the blocking section decreases as the diameter of the blocking section increases, the effect of the barrel section is more significant, and the effect of the blocking section is not obvious. Barrel deformation increases with the increase of transition section diameter, but it can be seen that the effect is not obvious.

$$M(x) = 1.58 - 0.6493A + 0.0254B + 0.0025C - 0.0029AB - 0.0004AC - 0.001BC + 0.2151A^2 + 0.0016B^2 + 0.0081C^2 \quad (3)$$

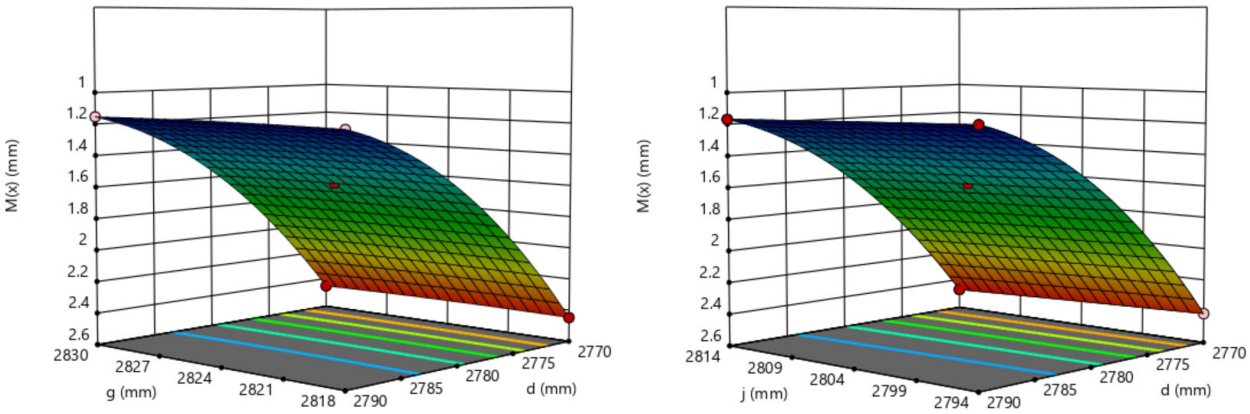

Figure 6. Relationship between design parameters and barrel deformation under static structure

From Figure 6, it can be seen that the cylinder deformation decreases as the diameter of the cylinder segment increases, and the change in the diameter of the transition and segment segments has little effect on the static structural deformation of the cylinder.

3.2.2. Test of response surface model

Table 4. $D(x)$ Response surface equation analysis of variance

Source	Sum of Square	df	Mean Square	F-value	p-value
Model	1.890E+09	9	2.100E+08	2.520E+07	<0.0001
A	1.140E+09	1	1.140E+09	1.368E+08	<0.0001
B	7.359E+08	1	7.359E+08	8.831E+07	<0.0001
C	1.376E+07	1	1.376E+07	1.651E+06	<0.0001
AB	25	1	25	3	0.1817
AC	25	1	25	30.1817	0.1817
BC	0	1	0	0	1
A^2	914.24	1	914.24	109.71	0.0019
B^2	700	1	700	84	0.0027
C^2	14.29	1	14.29	1.71	0.2817
Residual	25	3	8.33	-	-
Total	1.890E+09	12	-	-	-

Table 5. $S(x)$ Response surface equation analysis of variance

Source	Sum of Square	df	Mean Square	F-value	p-value
Model	0.0885	9	0.0098	25.46	0.0111
A	0.0728	1	0.0728	188.49	0.0008
B	0.0005	1	0.0005	1.37	0.3266
C	0.0011	1	0.0011	2.86	0.1893
AB	0.0029	1	0.0029	7.55	0.0708
AC	0.0001	1	0.0001	0.1817	0.6945
BC	2.25E-06	1	2.25E-06	0.0058	0.9440
A^2	0.0081	1	0.0081	20.96	0.0196
B^2	2.286E-06	1	2.286E-06	0.0059	0.9435
C^2	1.286E-06	1	1.286E-06	0.0033	0.9576
Residual	0.0012	3	0.004	-	-
Total	0.0896	12	-	-	-

Table 6. $M(x)$ Response surface equation analysis of variance

Source	Sum of Square	df	Mean Square	F-value	p-value
Model	3.52	9	0.3907	1.058E+06	<0.0001
A	3.37	1	3.37	9.136E+06	<0.0001
B	0.0052	1	0.0052	13994.66	<0.0001
C	0.0001	1	0.0001	138.16	0.0013
AB	0	1	0	92.70	0.0024
AC	4.9E-07	1	4.9E-07	1.33	0.3328
BC	1E-08	1	1E-08	0.0271	0.8797
A^2	0.1058	1	0.1058	2.865E+05	<0.0001
B^2	5.58E-06	1	5.58E-06	15.12	0.0302
C^2	0.0001	1	0.0001	404.97	0.0003
Residual	1.107E-06	3	3.692E-07	-	-
Total	3.52	12	-	-	-

The ANOVA results of the quadratic response surface models for $D(x)$, $S(x)$, and $M(x)$ are shown in Tables 4, 5, and 6. For the precision analysis of the models, the significance test values of model terms with p<0.05 indicate that the model relationships are significant, and those with p<0.01 indicate that the model relationships are highly significant. $D(x)$, $S(x)$, and $M(x)$ have F-values of 2.250E+07,25.46, and 1.058E+06, respectively, and correspond to the p-value is much less than 0.05, indicating that the optimized model has good significance.

The model is further tested for goodness of fit by using R^2 (coefficient of determination); the more the R^2 value tends to 1, the more the model matches the real situation. As the variables increase, the R^2 value also increases, which does not accurately reflect the true impact of the variables on the model, so an error analysis is performed using R^2_{adj} (corrected coefficient of determination).The formulas for F, R^2 and R^2_{adj} are as follows(4),(5),(6):

$$F = \frac{SS_R / k}{SS_E / (n-k-1)} = \frac{MS_R}{MS_E} \tag{4}$$

$$R^2 = \frac{\sum_{i=1}^{n} \left(yi - \hat{yi} \right)^2}{\sum_{i=1}^{n} \left(yi - \bar{y} \right)} \tag{5}$$

$$R^2_{adj} = 1 - \frac{n-1 \sum_{i=1}^{n} \left(yi - \hat{yi} \right)^2}{n-k-1 \sum_{i=1}^{n} \left(yi - \bar{y} \right)} \tag{6}$$

In the formula: n is the sample size;

k is the total number of variables of each order of the model can also be expressed as degrees of freedom;

yi is the experimental value;

$\bar{y}$ is the average of the experimental values;

$\hat{yi}$ is the response value obtained from the optimization model.

The closer the values of the correction coefficient R^2_{adj} and the prediction coefficient R^2 are to each other, while the closer they are to 1, the more reasonable the optimization model fits [8]. The analysis of the model coefficient of determination is shown in Table 7. it can be seen that the 2 values of the R^2 models are 1, 0.9871 and1, respectively, and are close to the values of R^2_{adj}, R^2 , indicating that the 2 models have a high degree of fit.

Table 7. Type determination coefficient analysis

Models	R^2	R^2_{adj}	*Adeq Precison*
$D(x)$	1	1	17006.3499
$S(x)$	0.9871	0.9483	14.2021
$M(x)$	1	1	2532.218

4. Multi-objective Optimization Results Analysis

Multi-objective genetic algorithm (MOGA), as a global optimization algorithm, has a strong global search capability and can obtain a series of Pareto frontier solution sets, so it is widely used in multi-objective optimization problem solving.

In order to ensure the convergence and accuracy of MOGA, the maximum allowable Pareto percentage is set to 70%, the convergence stability percentage is set to 2%, and the maximum number of iterations is set to 20. The trends of the rotary kiln stall thicknesses during the optimization search are shown in Figures 7 to 9.

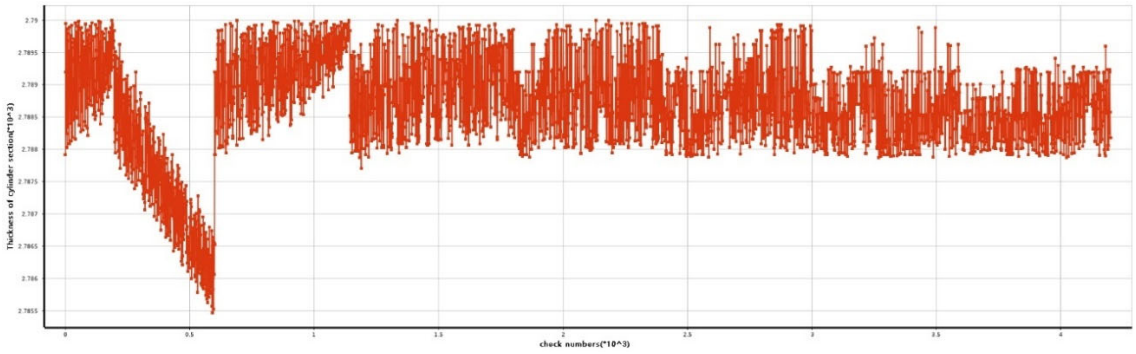

Figure 7. Trends in the optimization process of the thickness of the cylinder section

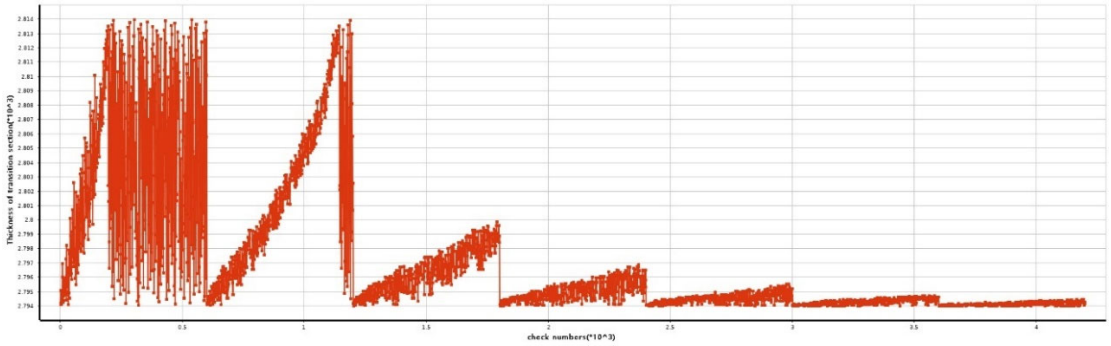

Figure 8. Trend of transition section thickness during the optimization process

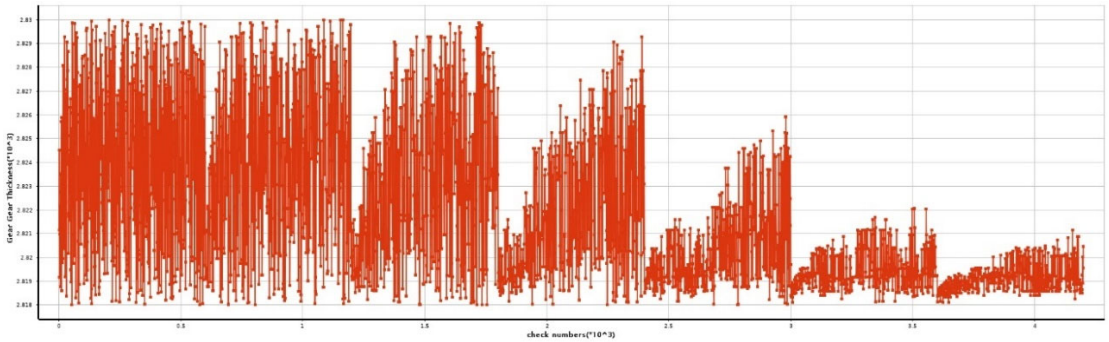

Figure 9. Trends in the process of optimization of the thickness of gear segments

Setting the number of candidate points as 3, 3 sets of Pareto optimal solutions are finally obtained after the iterative process in the above figure, as shown in Table 8.

Table 8. Pareto optimal solution

Optimization variables	Diameter of cylinder section d (mm)	Transition section diameter j (mm)	Gear section diameter g (mm)	Quality (kg)	Maximum deformation of static structure cylinder (mm)	Thermal structure coupling cylinder maximum deformation (mm)
Initial Value	2790	2814	2830	154750	1. 1755	73. 245
Candidate point 1	2790	2794	2819. 4	133230	1. 1254	73. 321
Candidate point 2	2790	2794	2820. 2	133420	1. 124	73. 326
Candidate point 3	2789. 9	2794	2819. 6	133240	1. 126	73. 315

4.1. Analysis of optimization results

After rounding, the optimized variables were finally d =2790 , j =2794 , g =2820 , and the optimal size was re-modeled and analyzed as the design size of the rotary kiln cylinder diameter, and the optimized stress-strain cloud diagram of the rotary kiln cylinder was obtained figure10 and figure11. The comparison of rotary kiln cylinder diameter parameters before and after optimization is shown in Table 9. According to the finite element results of the optimized rotary kiln barrel, the mass of the rotary kiln barrel is 133,380 kg , and the location of the maximum stress of the thermal structure coupling has been changed from the third position to the first value of 139.93 MPa , and the maximum stress of the static structure is 14.007 MPa . The maximum deformation of the static structure and thermal structure coupling is 1.1211 mm and 73.323 mm . Compared with the original model, the mass of the rotary kiln cylinder and the maximum deformation of the static structure are reduced, and the maximum deformation of the thermal structure coupling is increased, but the increase has almost no effect on the whole cylinder. The maximum stress of the static and thermal structure coupling increases, but it is still less than the yield limit of σ_{max} =345 and within the safe range, so the lightweight design of the rotary kiln cylinder is achieved.

Table 9. Comparison of parameters of rotary kiln barrel before and after optimization

Optimization variables	Diameter of cylinder section d (mm)	Transition section diameter j (mm)	Gear segment diameter g (mm)	Quality (kg)	Static structure maximum stress (Mpa)	Maximum deformation of static structure (mm)	Thermal structure coupling maximum stress (Mpa)	Maximum deformation of thermal structure coupling (mm)
Before optimization	2790	2814	2830	154750	10.149	1.1755	133.6	73.245
After optimization	2790	2794	2820	133380	13.872	1.1211	139.93	73.323

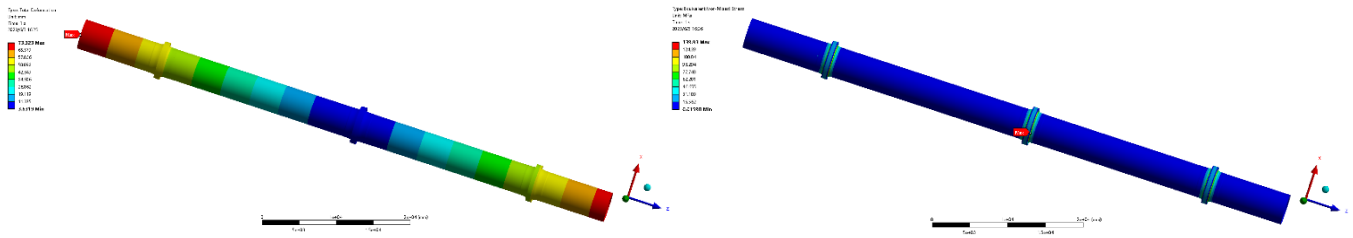

Figure 10. Maximum deformation and maximum displacement under the optimized thermal structure coupling

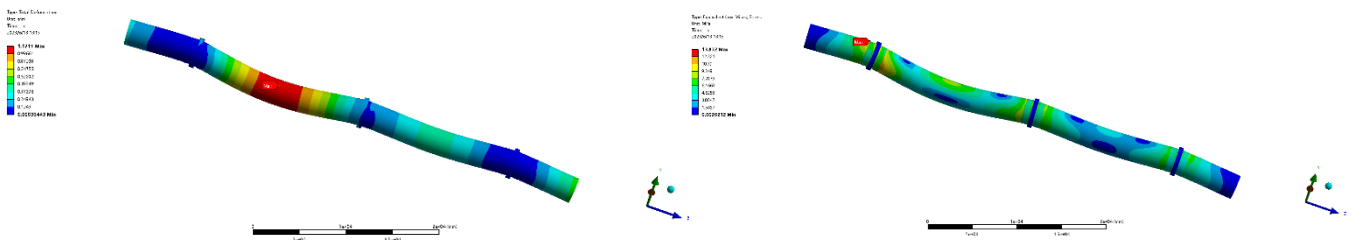

Figure 11. Maximum deformation and maximum displacement of the optimized static structure

5. Conclusion

Firstly, the structural parametric modeling of the rotary kiln equipment was carried out, and then the model was subjected to coupled finite element static structure and thermal structure analysis to obtain the maximum displacement and maximum deformation values and locations. The response surface function between the diameter parameters of the rotary kiln and the values of $D(x)$, $S(x)$, $M(x)$ was established by the response surface method, which was verified to have high prediction accuracy. The multi-objective genetic algorithm was used to find the optimal design parameters for the constructed model, and three sets of Pareto optimal solutions were obtained, and then the obtained three sets of solutions were compared to select the best structural parameters. The optimized structural parameters were re-modeled and finite element analyzed, and the results showed that the maximum deformation position of the optimized rotary kiln equipment was unchanged and the maximum stress position was changed; the deformation of the cylinder was reduced by 4.3% and the mass was reduced by 13.6% under the static structure, and although the maximum stress was increased, it was much smaller than the yield strength of the material and had a high safety margin. The optimized cylinder mass, maximum stress and maximum deformation under static structure, maximum deformation and maximum stress under thermal structure coupling are in good agreement with the numerical test results, and the deviation is within 1%, which proves the effectiveness of the optimized design method of rotary kiln cylinder device, and greatly improves the performance of rotary kiln cylinder and reduces the production cost, and provides a good solution for the rotary kiln This method has proved the effectiveness of the optimized design of rotary kiln cylinder device, greatly improved the performance of rotary kiln cylinder and reduced the production cost, and provided a reference for the research of optimized design of rotary kiln cylinder thickness.

References

[1] Xiao Yougang,Liu Yilun,Ma Aichun. Unsteady heat transfer model of rotary kiln wall and optimization of kiln skin thickness[J]. Chinese Journal of Nonferrous Metals, 2006, (6): 1115-1119.

[2] Li ZG, Hu GL, Jia Huifang, et al. Coaxial optimization of large rotary kiln with equal load based on finite element analysis[J]. Mechanical Science and Technology, 2014, 33(8): 1197-1202.

[3] Yang W, Zou G, Li P, et al. Numerical simulation study on structural optimization of rotary kiln for vanadium-containing shale roasting_Yang Wei[J]. Mechanical Design, 2015, 32(7): 101-104.

[4] Chen, M.F.. Finite element analysis of stress and strain in the support part of large rotary kiln_Chen M.F.[J]. Mechanical Design and Manufacture, 2014, (6): 62-64.

[5] Li Yanmin, Qin Shuqi, Li Kun, et al. Optimization and analysis of the number of supporting gears of rotary kiln[J]. Mining Machinery, 2018, 46(8): 59-64.

[6] Lei Xianming,Xiao Yougang,Chen Guoxin,et al. Optimization of rotary kiln cylinder fatigue resistance under multi-body discontinuous contact[J]. Journal of Sichuan University (Engineering Science Edition), 2014, 46(6): 185-190.

[7] Lei Xianming,Xiao Yougang,Chen Guoxin. Analysis of mechanical properties of rotary kiln cylinders under multi-body discontinuous contact[J]. Light Metals, 2015, (2): 9-13.

[8] Qiao B,Geng WD,Liu XC,et al. Development and design of large span two-stage rotary kiln_Qiao Bin (1) [J]. Mining Machinery, 2022, 50(12): 52-55.

[9] Wang Hehui, Xie Kedi, Chen Yifan, et al. Analysis of mechanical behavior of large rotary kiln cylinder structure[J]. Mechanical Strength, 2010, 32(4): 606-616.

[10] Li L, Zhang S, He Q, et al. Application of response surface methodology in experimental design and optimization[J]. Laboratory Research and Exploration, 2015, 34(8): 41-45.

[11] Ma QY, Tian A-L, Zhao Y-S, et al. Structural design optimization of SPS chimney based on Box-Behnken response surface method[J]. Naval Science and Technology, 2021, 43(17): 37-43.

[12] Wang J, Wang K, Lu S, et al. Optimization of TA5 titanium alloy process parameters based on response surface methodology[J]. Rare Metal Materials and Engineering, 2022, 51(6): 2130-2136.

[13] Xu, S. H., Zhang, G., Yang, X. P., et al. Optimization of heavy-duty robotic arm design based on response surface methodology[J]. Manufacturing Automation, 2022, 44(4): 70-72, 98.

[14] Li Weimin, Pan Shichao. Lightweight optimization design and research for damper spring seat[J]. Modern Manufacturing Engineering, 2022, (7): 142-148.

[15] Yang F, Wang Q, He GY, et al. Lightweight design of missile tail based on response surface optimization[J]. Journal of Ballistic Arrow and Guidance, 2022, 42(6): 79-84.

[16] Deng LJ, Wang SHX, Yang FQ. Optimized design for crashworthiness and light weight of automobile front bumper[J]. Modern Manufacturing Engineering, 2021, (8): 64-69.